Symbiotic Bacterial Metabolites Regulate Gastrointestinal Barrier Function via the Xenobiotic Sensor PXR and Toll-like Receptor 4

Madhukumar Venkatesh,[1,10] Subhajit Mukherjee,[1,10] Hongwei Wang,[1] Hao Li,[1] Katherine Sun,[2] Alexandre P. Benechet,[3] Zhijuan Qiu,[3] Leigh Maher,[3] Matthew R. Redinbo,[4] Robert S. Phillips,[5] James C. Fleet,[6] Sandhya Kortagere,[7] Paromita Mukherjee,[1] Alessio Fasano,[8] Jessica Le Ven,[9] Jeremy K. Nicholson,[9] Marc E. Dumas,[9] Kamal M. Khanna,[3,*] and Sridhar Mani[1,*]

[1]Departments of Genetics and Medicine, Albert Einstein College of Medicine, Bronx, NY 10461, USA
[2]Department of Pathology, Montefiore Medical Center, Bronx, NY 10467, USA
[3]Department of Immunology, University of Connecticut Health Center, Farmington, CT 06030, USA
[4]Department of Chemistry, University of North Carolina, Chapel Hill, NC 27599, USA
[5]Department of Chemistry, University of Georgia, Athens, GA 30602, USA
[6]Department of Nutrition Science, Purdue University, West Lafayette, IN 47907, USA
[7]Department of Microbiology & Immunology, Drexel University College of Medicine, Philadelphia, PA 19129, USA
[8]Department of Pediatrics, MassGeneral Hospital for Children, Harvard Medical School, Boston, MA 02114, USA
[9]Section of Biomolecular Medicine, Division of Computational and Systems Medicine, Department of Surgery and Cancer, Faculty of Medicine, Imperial College London, Exhibition Road, South Kensington, London SW7 2AZ, UK
[10]Co-first author
*Correspondence: kkhanna@uchc.edu (K.M.K.), sridhar.mani@einstein.yu.edu (S.M.)
http://dx.doi.org/10.1016/j.immuni.2014.06.014

SUMMARY

Intestinal microbial metabolites are conjectured to affect mucosal integrity through an incompletely characterized mechanism. Here we showed that microbial-specific indoles regulated intestinal barrier function through the xenobiotic sensor, pregnane X receptor (PXR). Indole 3-propionic acid (IPA), in the context of indole, is a ligand for PXR in vivo, and IPA downregulated enterocyte TNF-α while it upregulated junctional protein-coding mRNAs. PXR-deficient ($Nr1i2^{-/-}$) mice showed a distinctly "leaky" gut physiology coupled with upregulation of the Toll-like receptor (TLR) signaling pathway. These defects in the epithelial barrier were corrected in $Nr1i2^{-/-}Tlr4^{-/-}$ mice. Our results demonstrate that a direct chemical communication between the intestinal symbionts and PXR regulates mucosal integrity through a pathway that involves luminal sensing and signaling by TLR4.

INTRODUCTION

Intestinal luminal contents (e.g., bacteria, food, metabolic by-products) are known to influence the gut barrier function through immune recognition (Clemente et al., 2012; Salzman, 2011). However, specific effects of microbial luminal metabolites on regulating epithelial innate immune homeostasis (e.g., epithelial barrier function) is incompletely characterized (Ashida et al., 2012). Indeed, disruption of epithelial barrier function is now emerging as an important mediator of intestinal inflammation (e.g., inflammatory bowel disease) (Fasano and Shea-Donohue,

2005; Maloy and Powrie, 2011; Xavier and Podolsky, 2007) as well as organ pathophysiology (e.g., allergy, diabetes, obesity, heart disease, arthritis, cognitive defects) (Gummesson et al., 2011; Islam and Luster, 2012; Mayer, 2011; Meier and Plevy, 2007; Turner, 2009).

Given that there are approximately 100 trillion bacteria in the intestines, their metabolic by-products and chemical repertoire are likely to be important mediators of yet-to-be-defined host phenotype (Rath and Dorrestein, 2012). Indeed, although dietary constituents have been shown to regulate barrier function, discrete mechanisms of microbial metabolites that regulate intestinal epithelial integrity remain elusive (Leavy, 2011). Because adopted orphan nuclear receptors are known signaling intermediates for certain host-bacterial metabolites (e.g., bile acids and farnesoid x receptor [FXR], dietary ligands and aryl hydrocarbon receptor [AhR]), we focused on pregnane X receptor (PXR), because its promiscuous ligand binding pocket might well be capable of accommodating diverse small bacterial metabolites (Watkins et al., 2001).

To test the hypothesis that elements of the host environment (i.e., symbiotic bacteria) regulate intestinal barrier function through PXR, we focused on exploring the functions of indole metabolites (e.g., Indole 3-propionic acid [IPA]), that are exclusively produced by intestinal commensal microbes (Wikoff et al., 2009). In mice, IPA synthesis appears linked to the intestinal commensal *Clostridium sporogenes* (Wikoff et al., 2009). In humans under homeostatic conditions, blood IPA and indole concentrations remain in micromolar and millimolar range, respectively, with intestinal concentrations predicted to be much higher (Bansal et al., 2010). To date the cellular target of IPA remains elusive. To determine whether IPA could potentially regulate intestinal barrier function through PXR, we performed a combination of in vitro, ex vivo, and in vivo studies of the effect of IPA on epithelial permeability and inflammation. The results

showed that IPA (in the presence of indoles) served as a likely physiologic ligand for PXR and downregulated enterocyte-mediated inflammatory cytokine tumor necrosis factor-α (TNF-α) while upregulating junctional protein-coding mRNAs. PXR-deficient ($Nr1i2^{-/-}$) mice exhibited a distinctly "leaky" intestinal epithelium pathology, whereas replacing PXR using bone marrow chimeras established that PXR must be present in non-hematopoietic compartments for normal intestinal inflammatory signals and barrier functions. Importantly, $Nr1i2^{-/-}$ intestinal cells exhibited upregulation of toll-like receptor 4 (TLR4). These molecular events, as well as overall defects in the epithelial barrier, were corrected in $Nr1i2^{-/-}Tlr4^{-/-}$ mice. Collectively, these results demonstrate that a direct chemical communication between the gastrointestinal symbionts and a specific nuclear receptor pathway control mucosal homeostasis.

RESULTS

Symbiotic Intestinal Bacteria-Derived IPA Regulates Intestinal Permeability and Inflammation through PXR

To simulate in vivo homeostatic conditions, we activated PXR using a combination of indole with its respective metabolites. Although IPA alone was a weak human PXR (hPXR) agonist (EC_{50} 120 μM, E_{max} 6.38-fold over control) (Figure 1A), IPA in combination with indole significantly activated hPXR (Figure 1B). Similar results were observed with indole 3 acetic acid (IAA) (Figure S1A available online) and supported by in silico docking studies (Figures S1B and S1C; Table S1). In contrast, mouse PXR (mPXR) was potently activated by IPA (EC_{50} 0.55 μM, E_{max} 18.84-fold over control) in vitro (Figure 1A) and induced PXR target gene transcription in vivo (Figures 1C and S1D). More importantly, although specific indoles have been shown to activate the AhR (Denison and Nagy, 2003), we were unable to demonstrate activation of AhR by IPA (Figure S1E).

We next examined effect of indoles on enterocyte inflammatory signals and barrier function. Importantly, differences between $Nr1i2^{-/-}$ and $Nr1i2^{+/+}$ mice were maintained when specifically assaying small intestinal permeability in vivo (Figures S1F and S1G) as well as using an in vivo multiphoton intravital microscopy (Figure S1H and Movies S1 and S2).

For critical validation of the ex vivo experiments demonstrating IPA effects on junctional regulators, we coadministered *C. sporogenes* to germ-free mice in the presence or absence of L-tryptophan (Figure 1D). We verified that *C. sporogenes* inoculation led to production of IPA in vivo (thus, it was assumed that indoles were present) (Figure 1E). Germ-free mice exposed to *C. sporogenes* had a significant reduction in FITC-dextran recovery from the serum and this was further reduced in the presence of L-tryptophan dosing (Figure 1F). The mice intestinal mucosa exposed to *C. sporogenes* demonstrated significant induction of PXR target genes (*Mdr1*, *Cyp3a11*, *Ugt1a1*), which was further augmented in the presence of L-tryptophan (Figure 1G).

IPA Regulates Intestinal Inflammation through PXR

To validate that IPA was driving the anti-inflammatory response in vivo directly via PXR, we exposed intestinal commensal-depleted $Nr1i2^{+/+}$ and $Nr1i2^{-/-}$ mice to live or heat-killed *C. sporogenes*. All mice were subsequently exposed to indomethacin (Figure 2A). We verified that only live *C. sporogenes*,

but not the heat-killed bacterial inoculation, led to production of IPA in vivo (Figure 2B). There was a significant reduction in the histologic injury and in mucosal myeloperoxidase (MPO) enzyme activity in $Nr1i2^{+/+}$, but not in $Nr1i2^{-/-}$, mice (Figures 2C and 2D). Furthermore, in these mice, intestinal mucosa exposed to the *C. sporogenes* had significant induction of PXR target gene (*Ugt1a1*) when compared to mice exposed to the heat-killed strain (Figure 2E). No such effects were observed in $Nr1i2^{-/-}$ mice (Figures 2B–2E).

The effects of *C. sporogenes* in vivo were directly validated using IPA administration by the oral route in both $Nr1i2^{+/+}$ and $Nr1i2^{-/-}$ mice. Although IPA effects could be non-target dependent based on the concentrations administered (i.e., nonspecificity of molecular targets based on the concentration of IPA), we chose to study at fixed dose of IPA using an inflammation-based barrier defect (indomethacin) model. In this model, $Nr1i2^{+/+}$ and $Nr1i2^{-/-}$ mice were administered IPA followed by indomethacin, and intestinal permeability was assessed. The rationale was that a defect in permeability was required in order to show the effect of IPA in both the wild-type and $Nr1i2^{-/-}$ mice. IPA dosing significantly reduced FITC-dextran permeability in $Nr1i2^{+/+}$ (Figure 2F), but not in $Nr1i2^{-/-}$ (Figure 2G), mice.

In an in vivo model of 3-deoxy-D-manno-octulosonic acid (KDO2)-lipid A (TLR4 ligand) intubation, which elicits inflammatory signals without disrupting the intestinal tissue architecture (see Experimental Procedures), there was no overt histologic evidence of inflammation (Figure S2A). However, TNF-α mRNA (Figure S2B), p38-MAPK phosphorylation (Figure S2C), and permeability to FITC-dextran (Figure S2D) were clearly induced after KDO2 treatment. In this model, at IPA concentrations that were achievable through oral gavage (Figure S2E), we found that IPA notably decreased TNF-α mRNA expression more in the $Nr1i2^{+/+}$ mice (3.73-fold) intestinal epithelium relative to $Nr1i2^{-/-}$ mice (1.72-fold) (Figure S2F). Together, these studies and the effects of IPA depletion in vivo (see Table S2; Figures S2G–S2I) establish PXR as an important enterocyte target of IPA.

$Nr1i2^{-/-}$ Mice Exhibit Enhanced Ultrastructural Defects that Directly Correlate with Increased Intestinal Permeability and Xenobiotic Toxicity

To study the function of PXR under steady-state conditions, we performed detailed histological analysis using 6- to 8-week-old $Nr1i2^{-/-}$ and $Nr1i2^{+/+}$ mouse intestines. Although gross features appeared unchanged, histological examination of the mucosa of $Nr1i2^{-/-}$ mice small intestines showed significant diminution of the villus-crypt ratio (Figure S3A), marked neutrophil infiltration, and increased MPO enzyme activity (Figure S3B). The data shown compare the jejunum (highest expression of PXR in the intestine) of $Nr1i2^{+/+}$ and $Nr1i2^{-/-}$ mice; data pertaining to other regions (i.e., duodenum, ileum) have similar trends (data not shown). Although subtle, these differences indicate that the small intestine of $Nr1i2^{-/-}$ mice might persist in a state of mild elevated stress that might culminate as overt inflammation when exposed to injurious insults. Indeed, we did not observe any significant changes in unfolded protein response (UPR) genes (UPR RT^2 ProfilerPCR Array, SABiosciences); however, a single gene, Serp1 mRNA, was induced 27-fold in $Nr1i2^{-/-}$ as compared with $Nr1i2^{+/+}$ mouse intestinal mucosa (data not
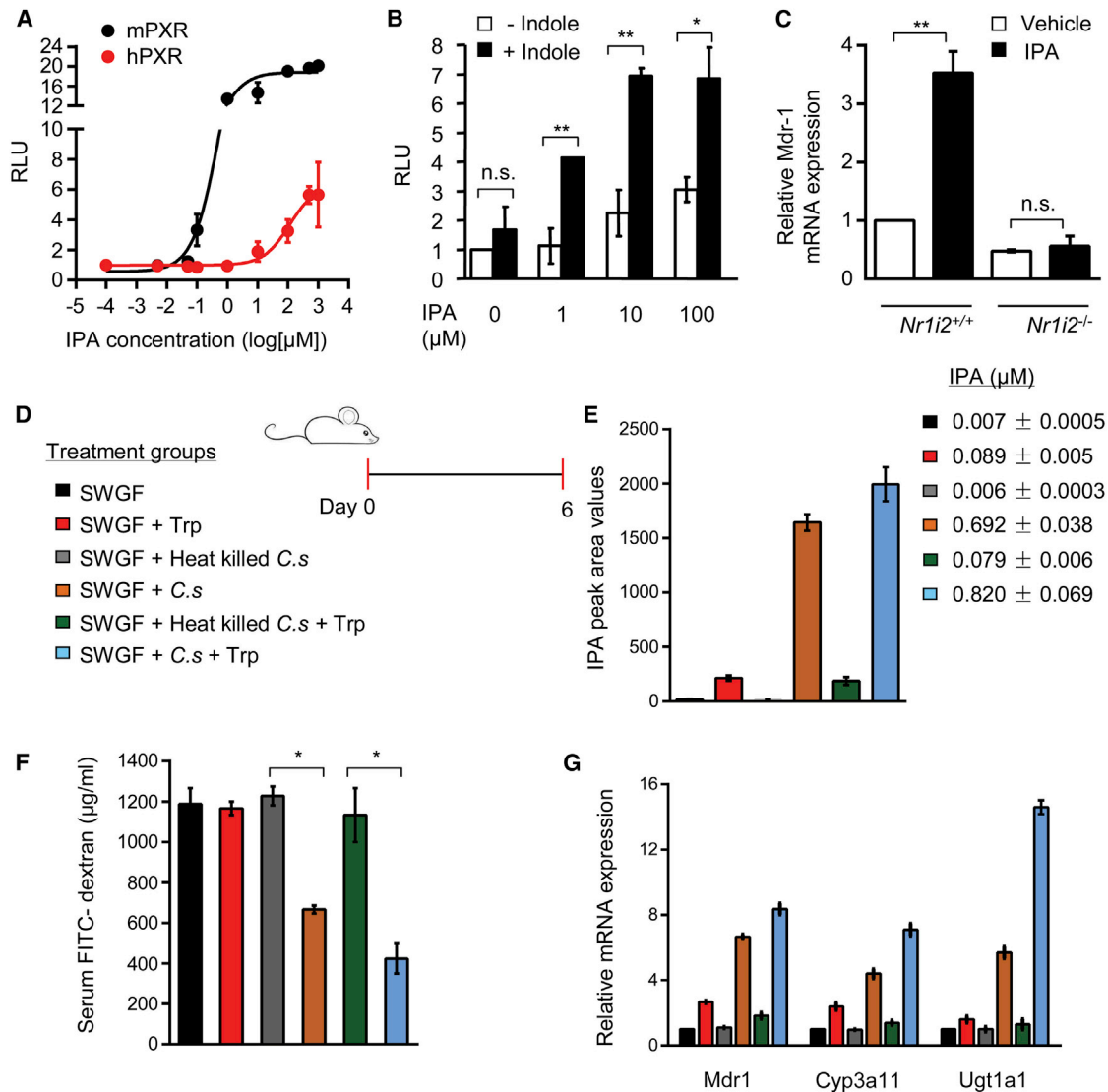
Figure 1. Commensal-Derived Indole Metabolite, IPA, Regulates PXR Activation

(A) Transcriptional activity of a PXR reporter gene (multidrug-resistance-associated protein 2 or MRP2 luciferase) cotransfected with mPXR (black) and hPXR (red) expression plasmids in 293T cells following treatment with IPA (n = 3). Abbreviation: RLU, relative light unit.

(B) Transcriptional activity of a PXR reporter gene (MRP2 luciferase) cotransfected with hPXR expression plasmid in 293T cells following treatment with fixed concentration of indole (1 mM) and increasing concentrations of IPA (n = 3). Abbreviation: RLU, relative light unit. Data expressed as fold change in RLU compared to vehicle (DMSO) controls.

(C) Real-time qPCR analysis of *Mdr1* expression in *Nr1i2*^{+/+} and *Nr1i2*^{−/−} mice jejunum villi enterocytes following oral treatment with IPA (20 mg/kg/day) (n = 5 per group). *p ≤ 0.0001; **p ≤ 0.001; n.s., not significant (two-way ANOVA with Tukey's multiple comparison test).

(D) Schematic of germ-free mouse treatment schedule. Six treatment groups are shown by color code: Swiss Webster Germ Free mice (SWGF) group, administered 100 μl LB and 100 μl sterilized water by oral gavage; SWGF + tryptophan (Trp) group, administered 100 μl LB + L-tryptophan; SWGF + Heat-killed *C. sporogenes* (*C.s*) group, administered *C.s* by oral gavage; SWGF + *C.s* group, administered *C.s* by oral gavage; SWGF + Heat-killed *C.s* + Trp group; and SWGF + *C.s* + Trp group, administered *C.s* and Trp by oral gavage (see Experimental Procedures). All the treatments were scheduled for 6 sequential days.

(E) Plasma IPA peak area intensity values plotted by treatment group as illustrated in the schema (D). Color-coded histograms show mean ± SEM values pertaining to each treatment group. IPA concentrations in micromoles (μM) are listed by color code.

(F) Serum FITC-dextran recovery in treatment groups illustrated in schema (D). *p ≤ 0.0001; two-way ANOVA with Tukey's multiple comparison test; n = 6 per group.

(G) Real-time qPCR analysis of Mdr1, Cyp3a11, and Ugt1a1 mRNA expression in small intestinal mucosa from schema (D).

All graphs show mean values ± SEM. Also see Figure S1, Table S1, and Movies S1 and S2.

shown). The induction of *Serp1* could act to stabilize membrane glycoprotein and stabilize their signaling (e.g., TLR4) (Yamaguchi et al., 1999). In keeping with the mild state of intestinal stress,

defects observed in *Nr1i2*^{−/−} mice are not due to any gross changes in proliferation (BrdU) or apoptosis (TUNEL) of the epithelium (Figure S3C).
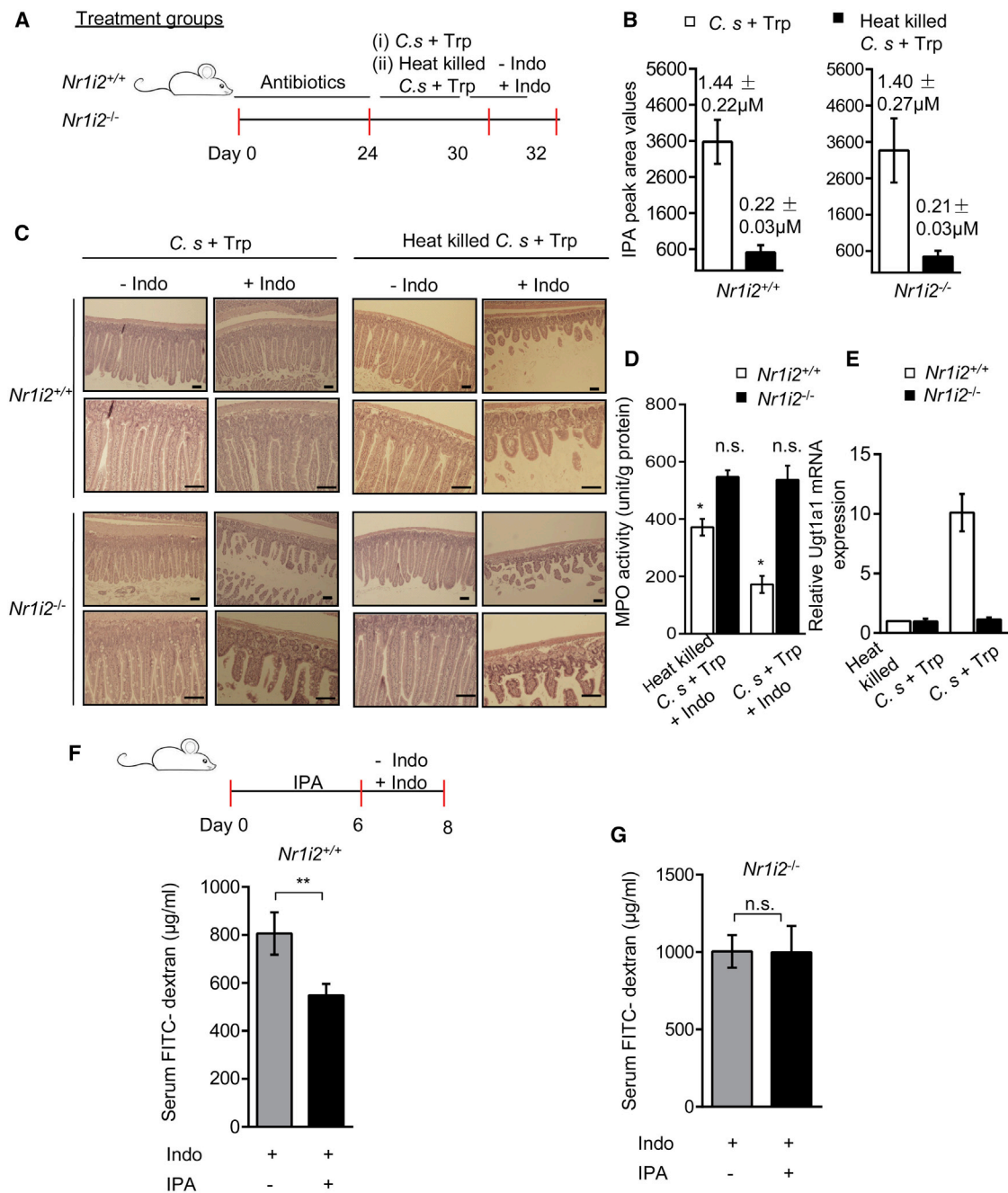
Figure 2. Commensal *C. sporogenes* Reconstitution Decreases Intestinal Permeability and Inflammation in a PXR-Dependent Manner in Mice

(A) Schematic of commensal depletion and *C. sporogenes* reconstitution experiment in $Nr1i2^{+/+}$ and $Nr1i2^{-/-}$ mice (see Experimental Procedures).

(B) Plasma IPA peak area intensity values plotted by treatment groups as illustrated in the schema (A). The IPA concentrations in micromoles (μM) pertaining to each group is illustrated above each histogram.

(C) Hematoxylin and eosin staining of *C. sporogenes* + L-tryptophan and heat-killed *C. sporogenes* + L-tryptophan exposed $Nr1i2^{+/+}$ and $Nr1i2^{-/-}$ mice jejunum cross-sections in accordance with schema (A). Scale bars represent 50 μm.

(D) Jejunal MPO activity (unit/g of total protein) in treatment groups from schema (A) as illustrated.

(E) Real-time qPCR analysis of *Ugt1a1* mRNA expression in small intestinal mucosa from schema (A).

(F and G) Serum FITC-dextran recovery following oral gavage of IPA (20 mg/kg/day) and indomethacin (see schematic) in (F) $Nr1i2^{+/+}$ (n = 9) and (G) $Nr1i2^{-/-}$ (n = 9) mice.

All graphs show mean values ± SEM. *p ≤ 0.01, two-way ANOVA with Sidak's multiple comparison test; n = 6 per group; **p ≤ 0.01, Student's t test; n.s., not significant. Also see Figure S2 and Table S2.
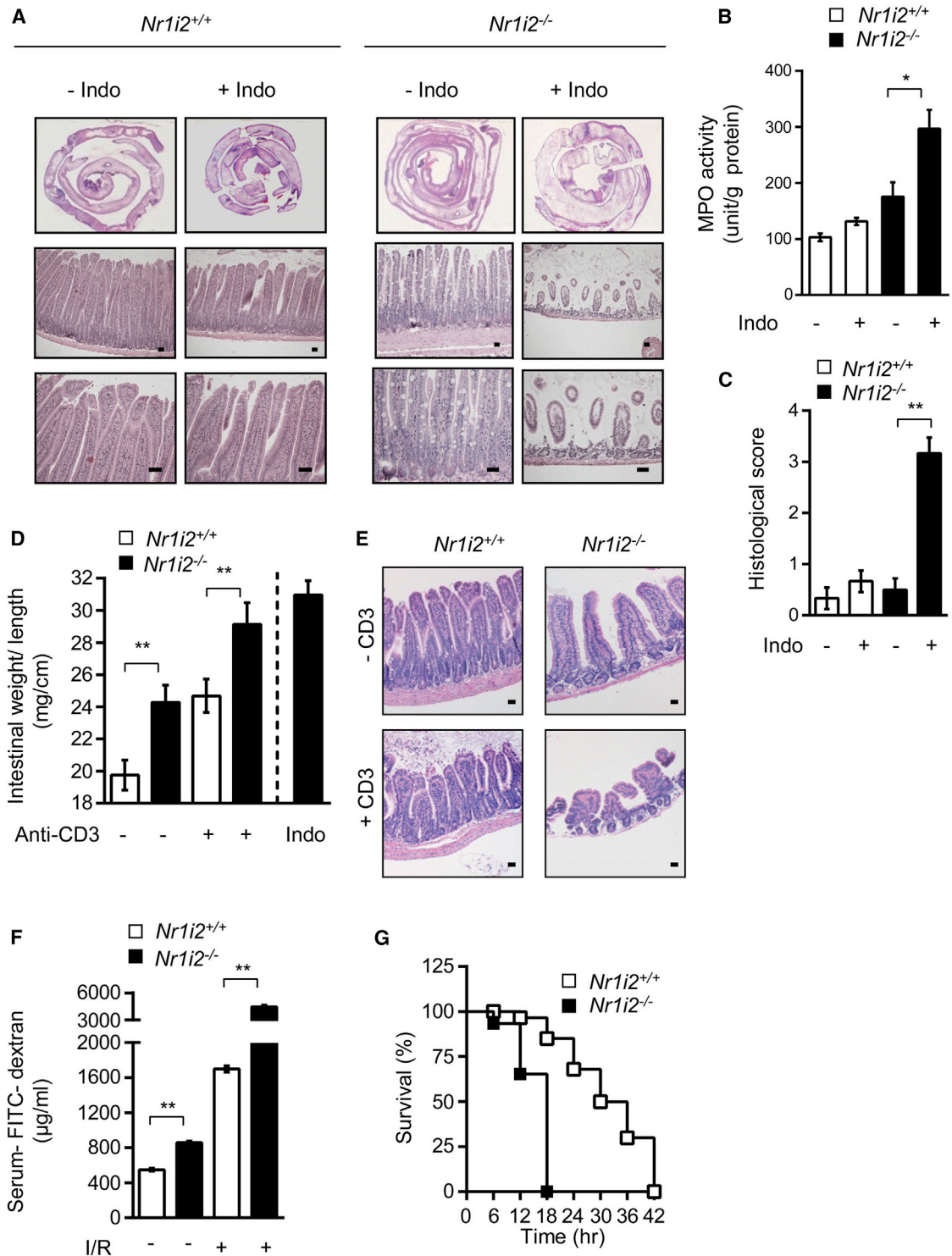
Figure 3. Nr1i2⁻/⁻ Mice Are More Susceptible to Toxic Injuries to the Small Intestine

(A) Hematoxylin and eosin staining of indomethacin (Indo)-treated $Nr1i2^{+/+}$ and $Nr1i2^{-/-}$ mice jejunum cross-sections.

(B) Jejunal MPO activity (unit/g of total protein) in $Nr1i2^{+/+}$ and $Nr1i2^{-/-}$ mice treated with indomethacin (n = 6 per group).

(C) Histological score measuring severity of tissue damage in jejunum from $Nr1i2^{+/+}$ and $Nr1i2^{-/-}$ mice in indomethacin-treated and untreated groups (n = 6 per group).

(D) Weight-to-length ratio of the jejunum (enteropooling) in $Nr1i2^{+/+}$ and $Nr1i2^{-/-}$ mice treated with anti-CD3 antibody. The change in weight-to-length ratio in $Nr1i2^{+/+}$ and $Nr1i2^{-/-}$ mice exposed to anti-CD3 was 27.6% and 22.9%, respectively. Values represent mean ± SEM (n = 5 per group).

(E) Hematoxylin and eosin staining of anti-CD3 antibody-treated $Nr1i2^{+/+}$ and $Nr1i2^{-/-}$ mice jejunum cross-sections.

(legend continued on next page)

To investigate whether PXR deficiency sensitizes mice to toxic insults, we subjected $Nr1i2^{-/-}$ and $Nr1i2^{+/+}$ mice to four toxic intestinal injury models. In the indomethacin-induced (85 mg/kg body weight, i.p., single dose) small intestine inflammation model, the $Nr1i2^{+/+}$ mice exhibited modest inflammation by histology (Figure 3A) and in jejunal MPO activity (Figure 3B). In contrast, the $Nr1i2^{-/-}$ mice showed significantly enhanced basal MPO activity, which increased upon indomethacin treatment (Figure 3B). In evaluating the histology in $Nr1i2^{-/-}$ mice, the histologic score increased by 6.2-fold over that observed in $Nr1i2^{+/+}$ mice (Figure 3C). In the anti-CD3 antibody-induced intestinal inflammation-edema model, mice were exposed to anti-CD3 (clone 2C11, 200 μg i.p.) and tissues were harvested 3 hr later for enteropooling. Notably, 100% of $Nr1i2^{-/-}$ mice given this dose of anti-CD3 antibody succumbed to intestinal edema and died within 72 hr of dosing. Indeed, small bowel isolated after 24 hr of dosing with anti-CD3 antibody showed that the mean values of enteropooling did not exceed 30 mg/cm (maximum value obtained ~31.5 mg/cm), suggesting that enteropooling values saturate at ~30–31 mg/cm (Musch et al., 2002). Although the changes in enteropooling values were not significantly different, it is clear that the $Nr1i2^{-/-}$ mice have increased susceptibility to anti-CD3-mediated injury based on the observation that the mean enteropooling values have maximized ~29.5 mg/cm (maximum value ~31.5 mg/cm) (Figure 3D). Therefore, the true increase in enteropooling is capped by saturated values in the anti-CD3-treated $Nr1i2^{-/-}$ mice. In addition, there was near-complete blunting of crypt-villus architecture in $Nr1i2^{-/-}$ as compared to $Nr1i2^{+/+}$ mice (Figure 3E). In the gastrointestinal ischemia-reperfusion model, the endogenous lectin complement pathway is a key initiator of intestinal inflammation in which the intestinal epithelium plays an important role in mediating such damage (Hart et al., 2005). An early finding that persists and then worsens with prolonged ischemia reperfusion is intestinal barrier dysfunction as manifested by changes in intestinal permeability (Hart et al., 2005). We assessed FITC-dextran recovery after oral gavage of $Nr1i2^{+/+}$ and $Nr1i2^{-/-}$ mice. The change in permeability as assessed by a change in recovery of mean levels of FITC-dextran in the serum of mice for $Nr1i2^{+/+}$ and $Nr1i2^{-/-}$ mice was 193% and 488.9% (Figure 3F), respectively. These results suggest that the $Nr1i2^{-/-}$ mice are significantly more susceptible to ischemia-reperfusion-mediated changes in intesinal barrier function. Finally, we used an endotoxic shock model, whereby systemic LPS induces a sepsis-like syndrome that prominently features intestinal barrier dysfunction (Roger et al., 2009). $Nr1i2^{-/-}$ mice treated with LPS had significantly worse survival than their $Nr1i2^{+/+}$ counterpart, suggesting that the loss of PXR significantly worsens survival in LPS-mediated septic syndrome, in which intestinal dysfunction plays a major role (Figure 3G). The LPS findings corroborate previous observations that PXR protects against LPS-mediated liver damage (Wang et al., 2010). Together, $Nr1i2^{-/-}$ mice demonstrate heightened sensitivity toward all four direct and indirect toxic intestinal injury models (Figure 3; Clayburgh et al., 2005; Ettarh and Carr, 1996; Zhou et al., 2006). The lack of significant steady-state gross inflammatory pathology in $Nr1i2^{-/-}$ mice contrasts with this heightened sensitivity toward xenotoxic challenge. To reconcile these findings, we performed ultrastructural and biochemical analysis of $Nr1i2^{+/+}$ and $Nr1i2^{-/-}$ mice jejunal epithelium. Transmission electron microscopy (TEM) of $Nr1i2^{-/-}$ mice intestinal epithelial cells showed loosely packed shorter microvilli relative to $Nr1i2^{+/+}$ mice (Figures 4A and 4B). Additionally, $Nr1i2^{-/-}$ mice microvilli show significantly diminished digestive enzyme activities compared to $Nr1i2^{+/+}$ microvilli (Figure 4C), and the activity (Figure 4D) and abundance (Figure 4E) of alkaline phosphatase is also notably reduced in the $Nr1i2^{-/-}$ mice intestine. Together, these data demonstrate that key aspects of the fine structure and enzyme expression in the $Nr1i2^{-/-}$ mice intestine would explain its enhanced sensitivity toward xenobiotic challenge (Matsui et al., 2011).

We next examined the cell-cell junctional complex, an essential structural component of the epithelial barrier. TEM showed that the tight-junction (Tj) and adherens-junction (Aj) complex (black arrow) in $Nr1i2^{-/-}$ mice intestinal epithelium was significantly more electron dense, diffuse with dense interconnected stranding (Figure 4F). The mRNA expression of these key junctional-complex markers were markedly diminished in the $Nr1i2^{-/-}$ mice, except Claudin-2, which is known to induce barrier defects (Figure 4G; Van Itallie and Anderson, 2006). Immunofluorescence showed similar trends (Figures S4A and S4B). Furthermore, in comparison with $Nr1i2^{+/+}$ mice, there is increased FITC-dextran recovery in serum (Figure 4H). Together, these ultrastructural and functional assays implicate PXR as a physiologic regulator of intestinal barrier function.

TLR4 Signaling Is an Essential Causative Pathway in the Epithelial Barrier Defects Observed in the $Nr1i2^{-/-}$ Mice

To screen for molecular mechanisms that are responsible for barrier dysfunction in $Nr1i2^{-/-}$ mice, we determined relative abundance of key host mRNAs encoding proteins involved in inflammation and microbial invasion. We performed real-time qPCR for anti-inflammatory, antimicrobial, and proinflammatory markers using total RNA isolated from $Nr1i2^{+/+}$ and $Nr1i2^{-/-}$ mice villi enterocytes. In the $Nr1i2^{-/-}$ mice, there is a significant downregulation of mRNAs involved in anti-inflammatory and antimicrobial function, along with a concomitant increase in proinflammatory cytokine mRNAs (Figure 5A). Given that TLRs are critical regulators of intestinal barrier function as well as inflammation, we chose to focus on them (Asquith and Powrie, 2010). We performed real-time qPCR for all ten mammalian (mouse) TLRs. TLR overexpression was modest (1.2- to 1.8-fold) and variable (Figure 5B); however, downstream TLR pathway kinase activation was enhanced in $Nr1i2^{-/-}$ mice (Figure S5A). Among the TLRs, TLR2 and TLR4 are expressed on the villi enterocytes and play significant roles in the regulation

(F) Serum FITC-dextran recovery following gastrointestinal ischemia-reperfusion injury in $Nr1i2^{+/+}$ and $Nr1i2^{-/-}$ mice (n = 5 per group). The change in permeability as assessed by a change in recovery of mean levels of FITC-dextran in the serum of $Nr1i2^{+/+}$ and $Nr1i2^{-/-}$ mice was 193% and 488.9%, respectively.

(G) Kaplan-Meier survival curves of $Nr1i2^{+/+}$ and $Nr1i2^{-/-}$ mice treated with LPS (n = 6 per group).

All graphs show mean values ± SEM. *p ≤ 0.02, **p ≤ 0.0001, two-way ANOVA with Tukey's multiple comparison test. Scale bars represent 50 μm. Also see Figure S3.
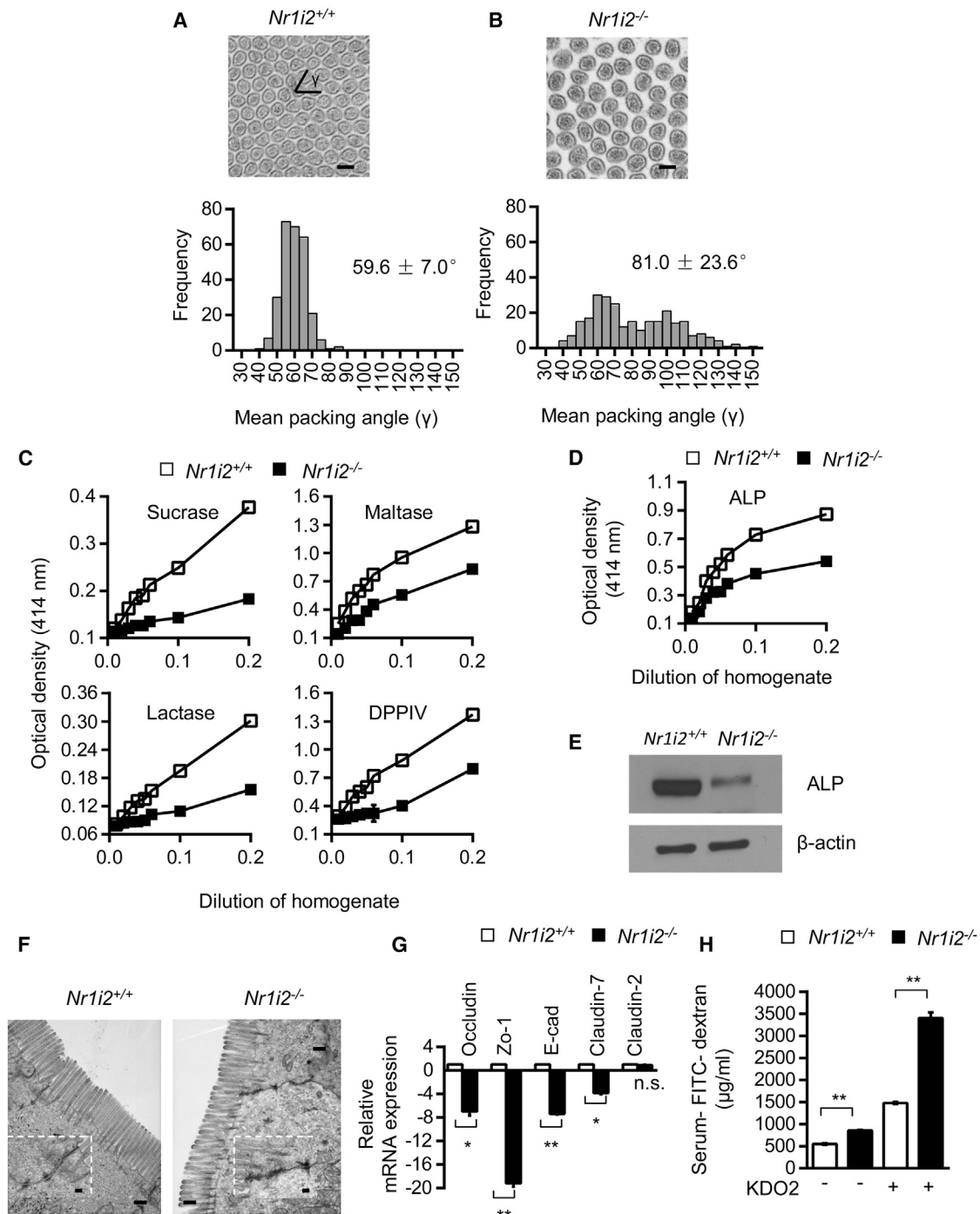
Figure 4. Ultrastructural and Functional Defects in *Nr1i2*^{−/−} Mice Small Intestine

(A and B) Representative TEM images of *Nr1i2*$^{+/+}$ (A) and *Nr1i2*$^{-/-}$ (B) mice jejunum shows loose packing of microvilli in *Nr1i2*$^{-/-}$ mice. γ represents packing angle between adjacent microvilli. Packing of microvilli in *Nr1i2*$^{+/+}$ and *Nr1i2*$^{-/-}$ mice jejunum was quantified by assessing the packing angle (γ) between adjacent microvilli. γ in *Nr1i2*$^{-/-}$ mice cross-sections (81.0° ± 23.6°, n = 273) is significantly higher and more variable compared to *Nr1i2*$^{+/+}$ mice (59.6° ± 7.0°, n = 275) (n = 5 per group).

(C) Sucrase, maltase, lactase, and dipeptidyl peptidase (DPPIV) enzyme activities in *Nr1i2*$^{+/+}$ and *Nr1i2*$^{-/-}$ mice jejunum villi enterocytes. Proportionality between amount of enzyme present (jejunal villi enterocyte homogenate containing 20 mg/ml of protein as enzyme, x axis) and amount of substrate liberated (optical density, y axis) in 60 min was plotted in the graph (n = 8–10 per group).

(D) Alkaline phosphatase enzyme activity in *Nr1i2*$^{+/+}$ and *Nr1i2*$^{-/-}$ mice jejunum villi enterocyte homogenate (n = 8–10 per group).

(E) Immunoblot analysis of alkaline phosphatase and β-actin (loading control) in *Nr1i2*$^{+/+}$ and *Nr1i2*$^{-/-}$ mice jejunum villi enterocytes (n = 5 per group).

(legend continued on next page)

of intestinal barrier function (Cario, 2010). To identify the TLRs that might affect inflammatory-cytokine-mediated barrier function in $Nr1i2^{-/-}$ mice, we incubated $Nr1i2^{-/-}$ enterocytes ex vivo with TLR2 and TLR4 inhibitors. TLR2 inhibition increased TNF-α and IL-6 mRNA expression in the intestinal mucosa of $Nr1i2^{-/-}$ mice; conversely, TLR4 inhibition significantly suppressed cytokine mRNA expression (Figure S5B). Furthermore, we generated $Nr1i2^{-/-}Tlr2^{-/-}$ mice and mucosa extracted from these mice show increased TNF-α and IL-6 mRNA expression when compared to $Nr1i2^{-/-}$ (Figure S5C). These findings correlate with the observation that the loss of $Tlr2$ in $Nr1i2^{-/-}$ mice increased intestinal permeability (Figures S5D–S5F).

We focused next on TLR4 because it is a critical determinant of LPS signaling in the intestine (Abreu et al., 2001). The basal expression of TLR4 protein was modestly elevated ($\sim$1.8-fold) in $Nr1i2^{-/-}$ (Figure 5C) and we also observed an inverse relationship between Pxr and Tlr4 mRNA expression in an intestinal cell line, Caco-2 (data not shown), and primary human intestinal mucosa (data not shown). To study the role of TLR4 in barrier dysfunction in $Nr1i2^{-/-}$ mice, we crossed the $Nr1i2^{-/-}$ with $Tlr4^{-/-}$ mice. In comparison with $Nr1i2^{-/-}$ mice, the abundance of mRNAs encoding key Tj, Aj proteins, and pro- and anti-inflammatory cytokines were reversed in $Nr1i2^{-/-}Tlr4^{-/-}$ mice epithelium to levels comparable to those observed in $Nr1i2^{+/+}$ mice (Figure 5D).

Because these markers encode for proteins involved in epithelial junctional complex formation and inflammation, we speculate that TLR4 is indeed responsible for the barrier dysfunction observed in $Nr1i2^{-/-}$ mice. To validate this hypothesis, we assessed whether the magnitude of TNF-α mRNA expression and FITC-dextran permeability was $Tlr4$ gene-dose dependent. We generated $Tlr4$ heterozygotes (at least $\sim$50% reduction in protein) in $Nr1i2^{-/-}$ mice background (data not shown). Enterocyte TNF-α mRNA expression and FITC-dextran recovery had similar quantitative reduction (Figures S5G and S5H). To further validate our observations regarding genes encoding junctional complex proteins, we performed TEM and immunofluorescence studies. The $Nr1i2^{-/-}Tlr4^{-/-}$ mice have microvilli lengths that were larger than $Nr1i2^{-/-}$ mice and comparable to that observed in $Nr1i2^{+/+}$ mice (Figure 5E). Indeed, the same trend was observed in the ultrastructure of the junctional complex (Figure 5F) and immunofluorescence staining for Zo-1 and E-cad (Figures S5I and S5J). The activities of brush border enzymes (Figure 5G) and FITC-dextran permeability (Figure 5H) in the $Nr1i2^{-/-}Tlr4^{-/-}$ mice was also similar to that observed in $Nr1i2^{+/+}$ mice. Additionally, $Nr1i2^{-/-}Tlr4^{-/-}$ mice displayed significantly attenuated damage response to indomethacin (Figures 6A and 6B). Together, these studies show that $Tlr4$ is essential to maintain epithelial barrier defects observed in the $Nr1i2^{-/-}$ mice.

IPA Protects against Indomethacin-Induced Intestinal Injury via PXR and TLR4

To further validate the requirement for TLR4 as a critical determinant of the effects of microbiota-derived PXR ligand IPA, $Tlr4^{+/+}$ and $Tlr4^{-/-}$ mice were exposed to IPA followed by indomethacin (as previously described for experiments with $Nr1i2^{+/+}$ and $Nr1i2^{-/-}$ mice). The results demonstrate that the presence of $Tlr4$ is required for IPA-induced changes in permeability defects induced by indomethacin (i.e., IPA significantly reduces FITC-dextran permeability induced by indomethacin) (Figure 6C). Indeed, to directly validate that the entire loop driven by microbiota-derived IPA results from modulation of TLR4, which in turn regulates intestinal permeability, $Nr1i2^{+/+}$ mice were commensal depleted for 15 days and/or followed by exposure to TLR4 ligand, KDO2, and/or IPA delivered orally (Figure 6D). The results demonstrate that commensal depletion increased intestinal permeability, which was further worsened by $\sim$2.8-fold with the addition of the TLR4 ligand KDO2. Note that in conventional $Nr1i2^{-/-}$ mice possessing intact intestinal microbiota (i.e., LPS), the FITC-dextran recovery in blood was $\sim$856 μg/ml (Figure 4H), which is actually lower than commensal-depleted $Nr1i2^{+/+}$ mice exposed to KDO2 ($\sim$1,495 μg/ml) (Figure 6D). In commensal-depleted $Nr1i2^{+/+}$ mice, reconstitution of mice with IPA results in a significant decrease in permeability. These results further validate our hypothesis that loss of microbiota producing IPA can induce a $Nr1i2^{-/-}$-like (not identical) state, whereby the presence of a TLR4 ligand, KDO2, worsens intestinal permeability and is corrected only when IPA is reconstituted in $Nr1i2^{+/+}$ mice (Figure 6D), but not in $Nr1i2^{-/-}$ mice (Figures 2F and 2G).

Finally, to understand whether the initial signals leading to disruption of the epithelial barrier originates via hematopoietic or nonhematopoietic cells (e.g., predominantly the epithelium), we performed bone marrow chimera experiments between $Nr1i2^{-/-}$ and $Nr1i2^{+/+}$ mice. These studies clearly show that immune reconstitution with either $Nr1i2^{+/+}$ or $Nr1i2^{-/-}$ hematopoietic cells have no effect on proinflammatory markers and intestinal permeability to FITC-dextran (Figures 7A–7C). Indeed, because intestine-homing hematopoietic-derived cells are major source of cytokines that disrupt barrier function (e.g., TLR4 signaling), it should be stated that PXR negatively regulates TLR4 bone-marrow-derived macrophages or mononuclear cells (data not shown). We saw no changes in serum FITC-dextran recovery, TNF-α, or IL-6 mRNA in $Nr1i2^{+/+}$ and $Nr1i2^{-/-}$ mice transplanted with either $Nr1i2^{-/-}$ or $Nr1i2^{+/+}$ bone marrow, respectively (Figures 7A–7C). In order to further determine whether there was any contribution by TLR4 signals emanating from hematopoietic-derived cells within the intestine, we derived combinatorial chimeric strains harboring loss or gain of TLR4 protein in these cells resident in $Nr1i2^{+/+}$ or $Nr1i2^{-/-}$ mice. $Nr1i2^{+/+}$ mice harboring either a gain or loss of TLR4 protein in

(F) Representative TEM images of $Nr1i2^{+/+}$ and $Nr1i2^{-/-}$ mice jejunum enterocytes demonstrating cell-cell junctional complexes and perijunctional cytoskeletal condensation. Inset shows magnified views of cell-cell junctional complex.
(G) Real-time qPCR analysis of key Tj and Aj regulatory genes in $Nr1i2^{+/+}$ and $Nr1i2^{-/-}$ mice jejunum villi enterocytes (n = 8–10 per group). Data plotted as fold change in $Nr1i2^{-/-}$ mice relative to mRNA levels in $Nr1i2^{+/+}$ mice.
(H) Serum FITC-dextran recovery in $Nr1i2^{+/+}$ and $Nr1i2^{-/-}$ mice following treatment with KDO2 (n = 8–10 per group).
All graphs show mean values $\pm$ SEM. *$p \leq 0.0001$; **$p \leq 0.0001$; n.s., not significant; two-way ANOVA with Tukey's multiple comparison test. Scale bars represent 0.5 μm (A, B, and F). Also see Figure S4.
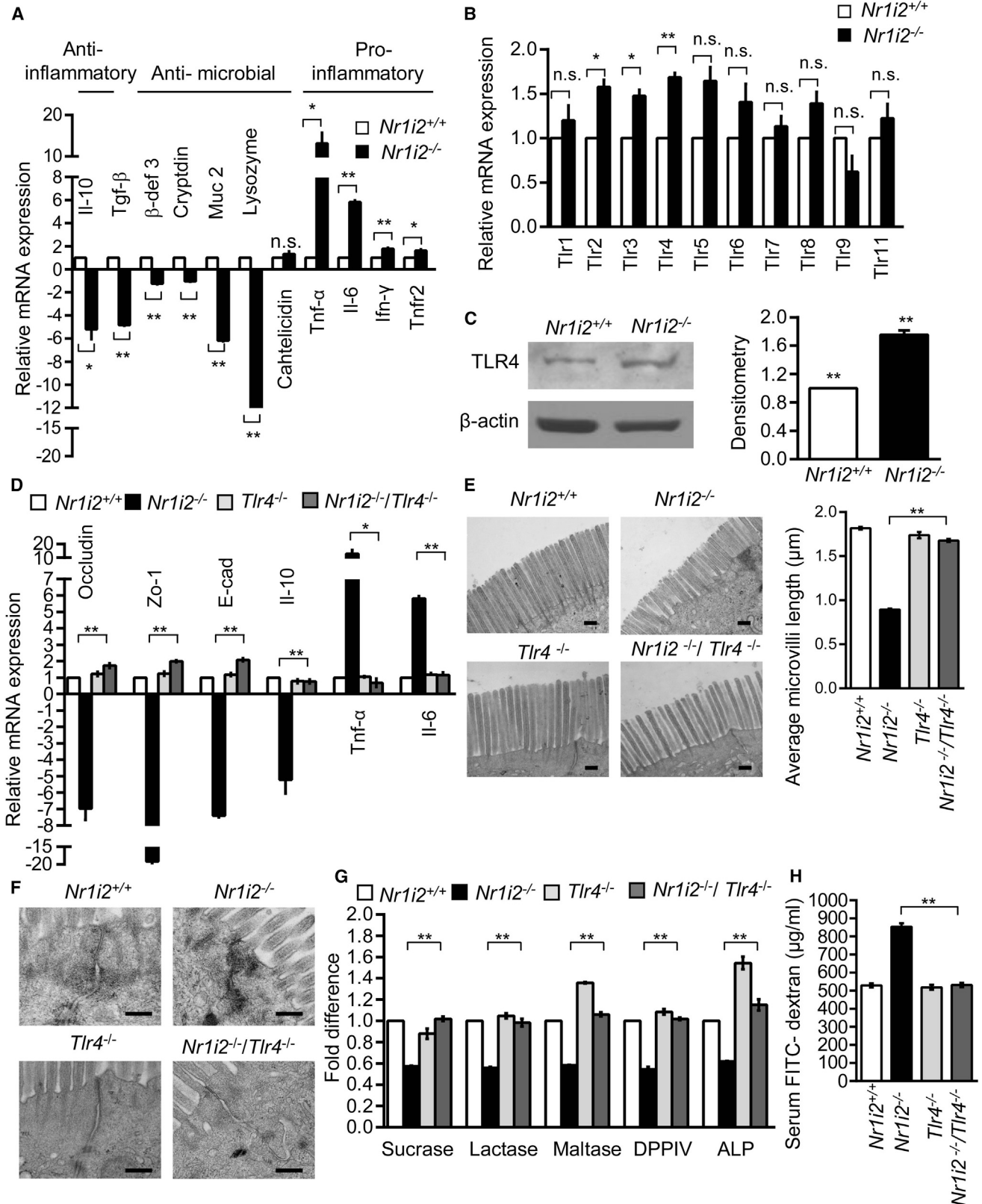
(legend on next page)

bone-marrow-derived cells within the intestine (LP cells) showed similar levels of serum FITC-dextran recovery as well as TNF-α or IL-6 mRNA, respectively. *Nr1i2*$^{-/-}$ mice expressing nonhematopoietic TLR4 and harboring either a gain or loss of TLR4 protein in bone-marrow-derived cells within the intestine (LP cells) showed no significant difference in serum FITC-dextran recovery or TNF-α or IL-6 mRNA levels. Similar results were obtained in *Nr1i2*$^{-/-}$ mice with loss of nonhematopoietic TLR4 and harboring either a gain or loss of TLR4 protein in bone-marrow-derived cells within the intestine (LP cells) (Figures 7D and 7E). This effectively shows that bone-marrow-derived TLR4, a major LPS-responsive effector of TNF-α, is unable to alter the intestinal phenotype induced by nonhematopoietic tissue. Thus, PXR resident in the nonhematopoietic compartment (i.e., epithelium) is important in dictating the initial response to external cues inciting epithelial barrier dysfunction.

DISCUSSION

The regulation of the intestinal barrier by intestinal commensal bacteria has been alluded to in several important reviews on this topic (Abreu, 2010; Salzman, 2011; Wells et al., 2011). However, thus far few discrete mechanisms have emerged (Abreu, 2010; Chen et al., 2010; Kelly et al., 2004; Patel et al., 2012). Our data support the role that PXR is an essential regulator of intestinal barrier effects under conditions of homeostasis. The four models of bowel injury, as well as evidence of chronic subclinical inflammation under basal conditions (Zhou et al., 2006), suggests that PXR is an essential modifier of innate immunity in the intestine and its response to xenobiotic injury. Both of these elements can be tied to intestinal barrier function, which is clearly aberrant in *Nr1i2*$^{-/-}$ mice (Matsui et al., 2011; Zhou et al., 2006). Bone marrow chimera studies indicate that neither *Nr1i2*$^{+/+}$ or *Nr1i2*$^{-/-}$ bone marrow alters expression of TNF-α, IL-6, and FITC-dextran recovery in mice of the opposite genotype, which strongly indicates that PXR expression in the nonhematopoietic compartment determines the epithelial phenotype. Because PXR is expressed predominantly in epithelial and not mesenchymal cells (Bookout et al., 2006), it is logical to conclude that the state of activation of epithelial PXR is paramount in determining the initial events leading to the observed intestinal barrier phenotype. Indeed, villus expression of PXR within the intestinal mucosa puts this receptor in nearest contact with the bacterial commensals in the lumen. A notable caveat in our experiments

was that in order to demonstrate the plausibility that indoles would have a physiologic target in vivo, we performed all our experiments using ex vivo systems (i.e., intestinal tissues incubated in OLA rather than in vivo administration). These experiments were performed ex vivo to circumvent the inherent problem associated with a perfect drug like OLA (PubChem, ST093573), which will probably be absorbed almost completely by mucosal surfaces, thus precluding efficient luminal delivery. In this context, germ-free mice (either gnotobiotic or axenic) would not be ideal experiments because only specific gut bacteria produce indoles and its metabolites (e.g., *C. sporogenes* in mice) (Wikoff et al., 2009). The exact species producing indoles and its metabolites in humans remain unknown; however, *C. sporogenes* is a soil bacterium present in humans and germ-free mice replete with this bacterium do show alterations in intestinal barrier function. Indeed, these results are consistent with and extend prior observations that germ-free mice reconstituted with conventional intestinal microbes significantly increase liver PXR and its target gene, *Cyp3a11*, expression (Claus et al., 2011). We have performed microbial reconstitution experiments in commensal-depleted mice that have validated our ex vivo observations that bacterial indoles (in particular IPA) directly affect intestinal barrier properties in vivo through actions mediated via PXR.

Our data implicate epithelial PXR as a central regulator of TLR4-mediated control of the intestinal barrier function. This regulation is intrinsically associated with intestinal commensals, specifically those involved with the metabolism of tryptophan and production of indoles and specific metabolites (i.e., IPA). We hypothesize that this association is tightly regulated to ensure "fine-tuning" of TLR4 expression in the intestine at levels appropriate to the abundance of LPS and perhaps other microbial-derived ligands. For homeostasis, all three components of this system (indole-secreting intestinal commensals, epithelial PXR expression, and TLR4) must be at appropriate levels for a given host—a lack of IPA or PXR or an excess of TLR4 can lead to intestinal barrier dysfunction. In fact, compromised intestinal barrier function has been implicated in the pathogenesis of several disease states (e.g., type I diabetes, asthma, autism, acne, allergies, etc.) including inflamatory bowel disease (IBD) (Gummesson et al., 2011; Islam and Luster, 2012; Mayer, 2011; Meier and Plevy, 2007; Turner, 2009). Hence, search for effective treatment options to prevent intestinal epithelial barrier defects may have broader implications beyond IBD.

Figure 5. Small Intestine Epithelial Barrier Dysfunction in *Nr1i2*$^{-/-}$ Mice Requires TLR4 Expression and Signaling

(A and B) Real-time qPCR analysis of (A) anti-inflammatory, antimicrobial, proinflammatory, and (B) *Tlr* gene expression in *Nr1i2*$^{+/+}$ and *Nr1i2*$^{-/-}$ mice jejunum villi enterocytes (n = 8–10 per group). Data plotted as fold change in *Nr1i2*$^{-/-}$ mice relative to mRNA levels in *Nr1i2*$^{+/+}$ mice.

(C) Immunoblot shows increased expression of TLR4 in *Nr1i2*$^{-/-}$ mice (n = 6 per group) (left). Immunoblots are representative of three independent experiments. Quantitation of band density was performed with two blots each with three different exposure times (right).

(D) Real-time qPCR analysis of key regulatory genes of epithelial barrier function in *Nr1i2*$^{+/+}$, *Nr1i2*$^{-/-}$, *Tlr4*$^{-/-}$, and *Nr1i2*$^{-/-}$*Tlr4*$^{-/-}$ mice jejunum villi enterocytes (n = 8–10 per group).

(E) Representative TEM images of *Nr1i2*$^{+/+}$, *Nr1i2*$^{-/-}$, *Tlr4*$^{-/-}$, and *Nr1i2*$^{-/-}$*Tlr4*$^{-/-}$ mice jejunum showing microvilli (left) and quantitation of average microvillus length (right).

(F) Representative TEM images of *Nr1i2*$^{+/+}$, *Nr1i2*$^{-/-}$, *Tlr4*$^{-/-}$, and *Nr1i2*$^{-/-}$*Tlr4*$^{-/-}$ mice jejunum showing cell-cell junctional complex.

(G) Enzyme (as denoted) activity assays performed with jejunal villi enterocyte homogenate from *Nr1i2*$^{+/+}$, *Nr1i2*$^{-/-}$, *Tlr4*$^{-/-}$, and *Nr1i2*$^{-/-}$*Tlr4*$^{-/-}$ mice. Data are expressed as fold change relative to *Nr1i2*$^{+/+}$ mice.

(H) Serum FITC-dextran levels in *Nr1i2*$^{+/+}$, *Nr1i2*$^{-/-}$, *Tlr4*$^{-/-}$, and *Nr1i2*$^{-/-}$*Tlr4*$^{-/-}$ mice (n = 8–10 per group).

All graphs show mean values ± SEM. *p ≤ 0.05; **p ≤ 0.01; n.s., not significant; two-way ANOVA with Tukey's multiple comparison test in (A), (B), (D), (E), (G), and (H) or Student's t test in (C). Scale bars represent 0.5 μm in (E) and (F). Also see Figure S5.
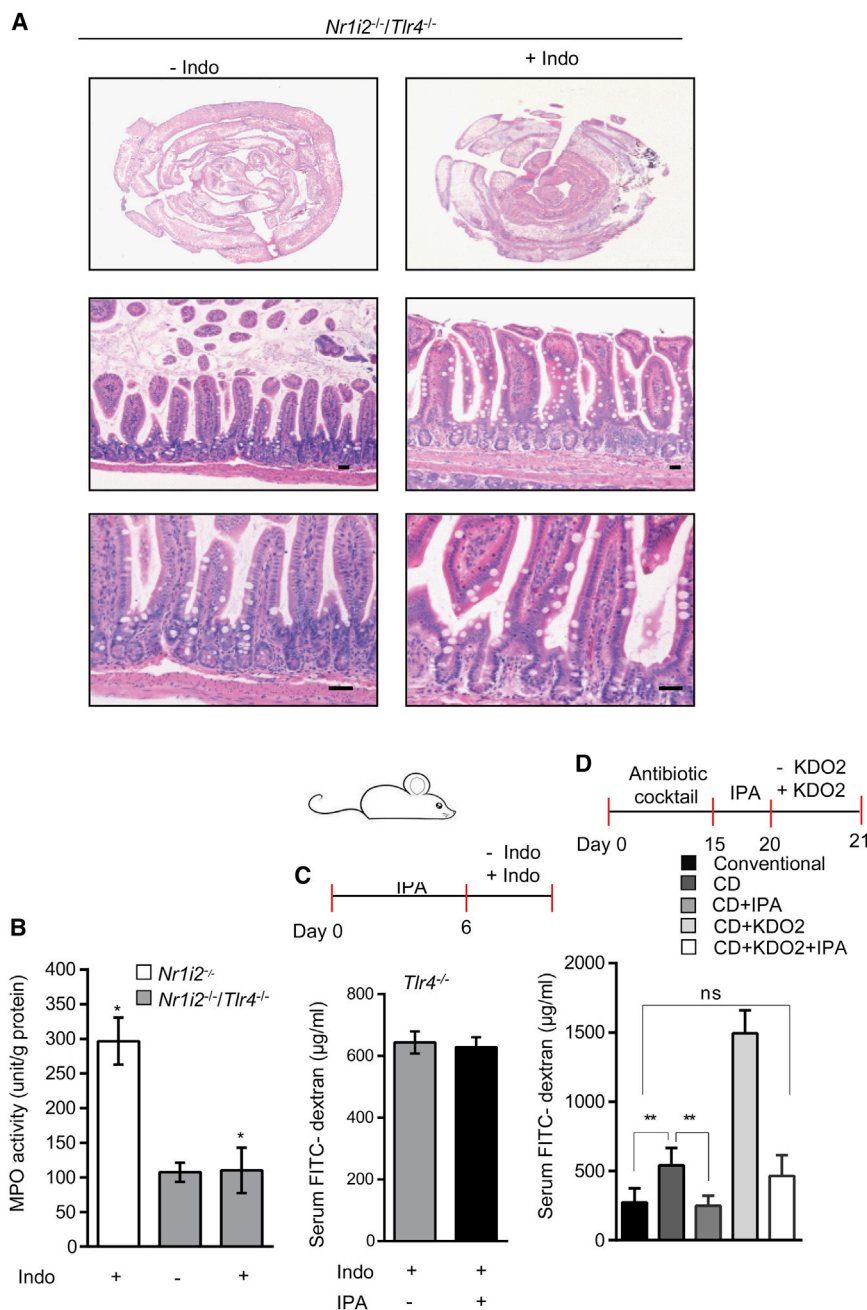
Figure 6. TLR4 Is Critical for Indomethacin-Induced Intestinal Injury as well as IPA Effects on Permeability In Vivo

(A) Representative hematoxylin and eosin staining of vehicle (-Indo) and indomethacin (Indo)-treated $Nr1i2^{-/-}Tlr4^{-/-}$ mice jejunum cross-sections (n = 6 per group).

(B) Jejunal MPO activity (unit/g of total protein) in $Nr1i2^{-/-}$ and $Nr1i2^{-/-}Tlr4^{-/-}$ mice treated with indomethacin (n = 6 per group). *$p \leq 0.005$, one-way ANOVA with Sidak's multiple comparison test.

(C) Serum FITC-dextran recovery following oral gavage of IPA (20 mg/kg/day) and indomethacin (see schematic) in $Tlr^{-/-}$ (n = 9) mice.

(D) Serum FITC-dextran recovery following oral gavage of IPA (20 mg/kg/day) and KDO2 200 μg/day (see schematic) in conventional mice ($Nr1i2^{+/+}$) and commensal-depleted (CD) mice ($Nr1i2^{+/+}$) (n = 8 per group).

All graphs show mean values ± SEM. *$p \leq 0.004$, **$p \leq 0.05$; n.s., not significant; two-way ANOVA with Tukey's multiple comparison test.

nine metabolites might be involved in the regulation of immune tolerance toward intestinal microbiota by inducing Treg cell differentiation that produce IL-10 (Lin et al., 2010). Furthermore, plasma tryptophan levels are reduced in patients with Crohn's disease (Gupta et al., 2012; Hisamatsu et al., 2012). Interestingly, fecal tryptophan levels are elevated in patients with Crohn's disease, suggesting perhaps that tryptophan metabolism is blunted in the microbiota of these patients (Jansson et al., 2009). In keeping with this notion of reduced tryptophan metabolism, indoxyl sulfate (product of indole metabolism by bacteria) is reduced in mice exposed to DSS (Dong et al., 2013) and IPA is significantly reduced in the *H. hepaticus* colitis model in $Rag2^{-/-}$ mice (Lu et al., 2012). Furthermore, patients with HIV infection demonstrate an inverse correlation of serum IPA and LPS (marker of intestinal microbial translocation), supporting the view that IPA regulates intestinal permeability in humans (Cassol et al., 2013). These observations are consistent with the notion that altered bacterial amino acid metabolism correlates with intestinal homeostasis (Martin et al., 2008). Thus, taken together, these observations provide important chemical biology steps toward a more comprehensive understanding of intestinal barrier function.

Moreover, our data in epithelial cells complement parallel nuclear-receptor-driven pathways in intestinal immune cells that regulate barrier function (Kelly et al., 2004; Leavy, 2011). It adds a new dimension to recent observations that the intestinal epithelial homeostasis is tightly orchestrated by the circadian clock (e.g., RevErbα) as well as microbiota transduced by TLRs (Mukherji et al., 2013) and that bacterially derived uracil serve as modulators of mucosal immunity and intestine-microbe homeostasis in *Drosophila* (Lee et al., 2013). Metabolomic analysis have identified low levels of tryptophan in $Il10^{-/-}$ mice, and its host-derived kyneurenine metabolite levels are elevated. These observations have led to the hypothesis that the kynure-

EXPERIMENTAL PROCEDURES

Cell Lines and Reagents

The human colon cancer cell lines (Caco-2 and LS174T) and 293T cells were obtained from the American Type Culture Collection (ATCC) and cultured
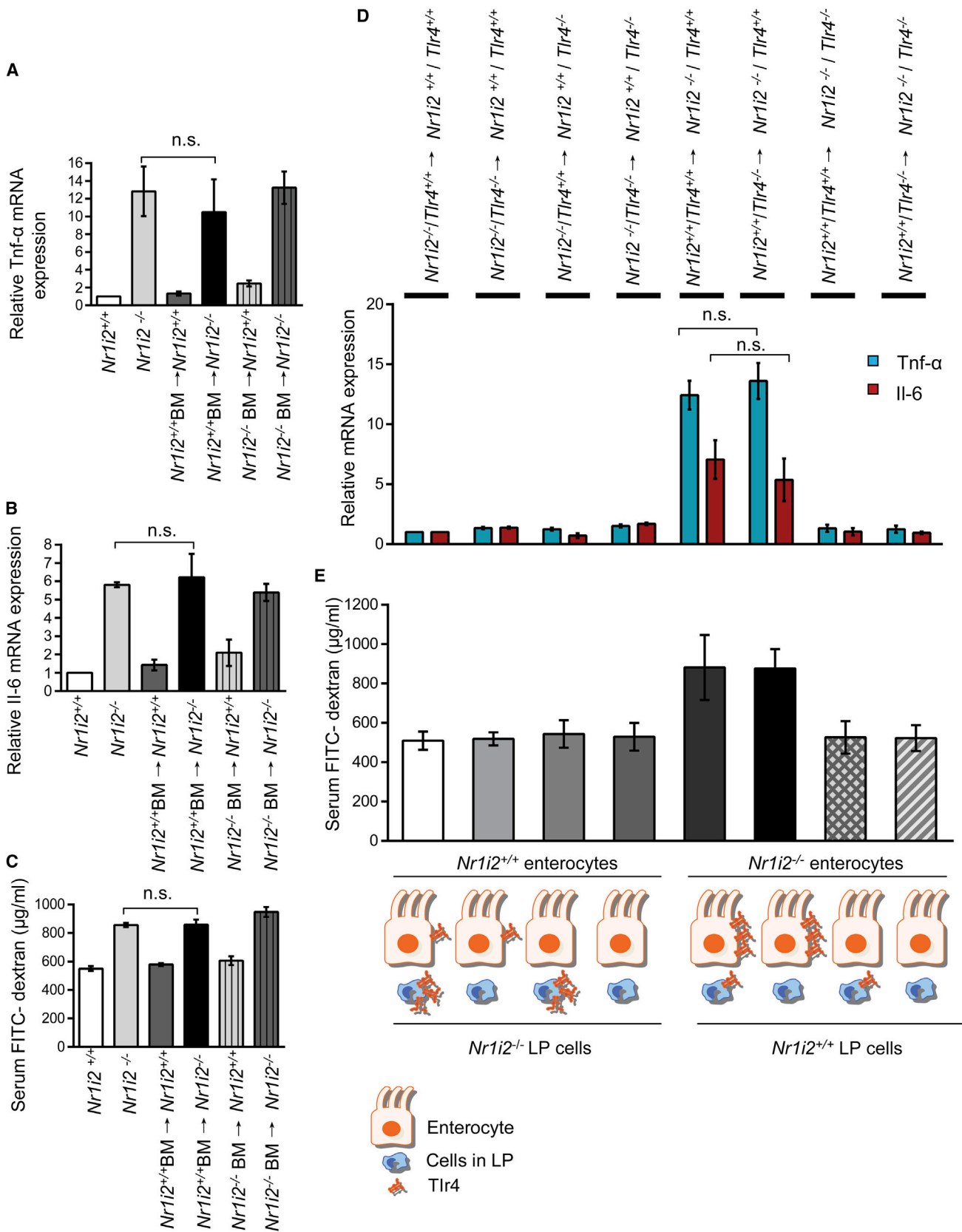
(legend on next page)

according to ATCC recommendations. For further details, see the Supplemental Experimental Procedures.

Mice

$Tlr4^{-/-}$ (B6.B10ScN-Tlr4$^{lps-del}$/JthJ, stock number 007227), $Tlr2^{-/-}$ (B6.129-Tlr2tm1Kir/J, stock number 004650), and C57BL/6J (stock number 000664) mice were obtained from the Jackson Laboratory. Swiss Webster (SW, control) and Swiss Webster Germ Free (SWGF) mice (7–8 weeks old, female) were purchased from Taconic. All animal experiments were approved by the animal institute committee (protocol # 20070715, 20100711) of the Albert Einstein College of Medicine and were performed in accordance with institutional and national guidelines. For further details, see the Supplemental Experimental Procedures.

Genotyping

Mouse tail DNAs were used for genotyping according to manufacturer's instructions (DNeasy Blood and Tissue kit, QIAGEN). Primer sequences and methods are in the Supplemental Experimental Procedures.

Histology and Immunofluorescence Analysis

Intestinal tissue sections (paraffin and frozen) were prepared and hematoxylin-eosin staining was performed in the histology core facility of Albert Einstein College of Medicine. Histological scoring was performed according to previously published methods (Asano et al., 2009). Experimental details in the Supplemental Experimental Procedures.

Isolation of Small Intestine Villi Enterocytes

We have employed the modified Weiser method to isolate pure villus enterocytes from the jejunum in all mice experiments as previously published (Weiser, 1973). Details in the Supplemental Experimental Procedures.

Oral Dosing of IPA

$Nr1i2^{+/+}$ and $Nr1i2^{-/-}$ mice were gavaged with 10, 20, and 40 mg/kg IPA, dissolved in sterile PBS (pH 7.4) in 100 μl volume per mice for 4 consecutive days. Swiss Webster (SW) and Swiss Webster Germ Free (SWGF) mice were orally gavaged with 20 mg/kg IPA for 4 consecutive days.

In Vivo Toxic Small Intestine Injury Models

For indomethacin-induced mouse jejunitis model, we have modified a protocol published by Ettarh and Carr (1996) by using a single intraperitoneal dose of indomethacin to reduce the toxicity in $Nr1i2^{-/-}$ mice. Details in the Supplemental Experimental Procedures.

Lenti-Based shRNA Knockdown Systems

Details of the procedure can be found in the recent publication by our laboratory (Wang et al., 2011).

Statistical Analysis

Data are shown as mean ± SEM. The significance of difference was analyzed by two-tailed Student's t test or ANOVA with post-hoc tests as indicated. The Kaplan-Meier method was used for survival and differences were analyzed by the log rank test (Figure 3G). All analyses were performed using GraphPad PRISM v.6.01 (GraphPad Software). $p < 0.05$ was considered statistically significant.

Further experimental details, including in vitro transcription assay, transmission electron microscopy, enzyme activity assay, tissue myeloperoxidase (MPA) activity assay, in vivo intestine permeability assay, germ-free mice, commensal depletion, real-time quantitative RT-PCR, immunoblot, tandem mass spectrometry (LC/MS/MS), bone marrow transplantation, BrdU and TUNEL staining, TLR2 and TLR4 inhibition experiments, and intravital imaging of the intestines, can be found in the Supplemental Experimental Procedures.

SUPPLEMENTAL INFORMATION

Supplemental Information includes Supplemental Experimental Procedures, five figures, two tables, and two movies and can be found with this article online at http://dx.doi.org/10.1016/j.immuni.2014.06.014.

AUTHOR CONTRIBUTIONS

S. Mukherjee, S. Mani, and M.V. designed the research; S. Mukherjee, M.V., H.W., A.P.B., Z.Q., L.M., H.L., and S.K. performed the experiments; R.S.P., A.F., and K.M.K. contributed new reagents, analytic tools, and/or concepts; J.L.V. performed and analyzed MS experiments; M.E.D. and J.K.N. analyzed MS data; J.L.V. and M.E.D. wrote the paper; and S. Mukherjee, J.C.F., M.R.R., P.M., M.V., and S. Mani analyzed the data and wrote the paper.

REFERENCES

Abreu, M.T. (2010). Toll-like receptor signalling in the intestinal epithelium: how bacterial recognition shapes intestinal function. Nat. Rev. Immunol. *10*, 131–144.

Abreu, M.T., Vora, P., Faure, E., Thomas, L.S., Arnold, E.T., and Arditi, M. (2001). Decreased expression of Toll-like receptor-4 and MD-2 correlates with intestinal epithelial cell protection against dysregulated proinflammatory gene expression in response to bacterial lipopolysaccharide. J. Immunol. *167*, 1609–1616.

Asano, T., Tanaka, K., Yamakawa, N., Adachi, H., Sobue, G., Goto, H., Takeuchi, K., and Mizushima, T. (2009). HSP70 confers protection against indomethacin-induced lesions of the small intestine. J. Pharmacol. Exp. Ther. *330*, 458–467.

Ashida, H., Ogawa, M., Kim, M., Mimuro, H., and Sasakawa, C. (2012). Bacteria and host interactions in the gut epithelial barrier. Nat. Chem. Biol. *8*, 36–45.

Figure 7. Epithelial Barrier Defects in $Nr1i2^{-/-}$ Mice Small Intestine Is Dependent on Nonhematopoietic Compartment
(A and B) Real-time qPCR analysis of proinflammatory markers (A) TNF-α and (B) IL-6 was assessed in $Nr1i2^{+/+}$ (n = 10), $Nr1i2^{-/-}$ (n = 10), $Nr1i2^{+/+}$ BM → $Nr1i2^{+/+}$ (n = 9), $Nr1i2^{+/+}$ BM → $Nr1i2^{-/-}$ (n = 9), $Nr1i2^{-/-}$ BM → $Nr1i2^{+/+}$ (n = 6), and $Nr1i2^{-/-}$ BM → $Nr1i2^{-/-}$ (n = 5) mice jejunal villi enterocytes. Data are expressed as fold change in all mice groups compared to $Nr1i2^{+/+}$ mice.
(C) In vivo FITC-dextran permeability assay was performed in $Nr1i2^{+/+}$ (n = 10), $Nr1i2^{-/-}$ (n = 10), $Nr1i2^{+/+}$ BM → $Nr1i2^{+/+}$ (n = 9), $Nr1i2^{+/+}$ BM → $Nr1i2^{-/-}$ (n = 9), $Nr1i2^{-/-}$ BM → $Nr1i2^{+/+}$ (n = 6), and $Nr1i2^{-/-}$ BM → $Nr1i2^{-/-}$ (n = 5) mice.
(D) Real-time PCR analysis of proinflammatory markers (blue) TNF-α and (red) IL-6 was assessed in genotypes illustrated (n = 5) mice jejunal mucosa. Data are expressed as fold change in all mice groups compared to $Nr1i2^{-/-}Tlr4^{+/+}$ → $Nr1i2^{+/+}Tlr4^{+/+}$ mice.
(E) In vivo FITC-dextran permeability assay was performed in (n = 5) mice jejunal mucosa.
All graphs show mean values ± SEM; n.s., not significant; two-way ANOVA with Tukey's multiple comparison test.

Asquith, M., and Powrie, F. (2010). An innately dangerous balancing act: intestinal homeostasis, inflammation, and colitis-associated cancer. J. Exp. Med. *207*, 1573–1577.

Bansal, T., Alaniz, R.C., Wood, T.K., and Jayaraman, A. (2010). The bacterial signal indole increases epithelial-cell tight-junction resistance and attenuates indicators of inflammation. Proc. Natl. Acad. Sci. USA *107*, 228–233.

Bookout, A.L., Jeong, Y., Downes, M., Yu, R.T., Evans, R.M., and Mangelsdorf, D.J. (2006). Anatomical profiling of nuclear receptor expression reveals a hierarchical transcriptional network. Cell *126*, 789–799.

Cario, E. (2010). Toll-like receptors in inflammatory bowel diseases: a decade later. Inflamm. Bowel Dis. *16*, 1583–1597.

Cassol, E., Misra, V., Holman, A., Kamat, A., Morgello, S., and Gabuzda, D. (2013). Plasma metabolomics identifies lipid abnormalities linked to markers of inflammation, microbial translocation, and hepatic function in HIV patients receiving protease inhibitors. BMC Infect. Dis. *13*, 203.

Chen, H.Q., Yang, J., Zhang, M., Zhou, Y.K., Shen, T.Y., Chu, Z.X., Zhang, M., Hang, X.M., Jiang, Y.Q., and Qin, H.L. (2010). *Lactobacillus plantarum* ameliorates colonic epithelial barrier dysfunction by modulating the apical junctional complex and PepT1 in IL-10 knockout mice. Am. J. Physiol. Gastrointest. Liver Physiol. *299*, G1287–G1297.

Claus, S.P., Ellero, S.L., Berger, B., Krause, L., Bruttin, A., Molina, J., Paris, A., Want, E.J., de Waziers, I., Cloarec, O., et al. (2011). Colonization-induced host-gut microbial metabolic interaction. MBio *2*, e00271–e10.

Clayburgh, D.R., Barrett, T.A., Tang, Y., Meddings, J.B., Van Eldik, L.J., Watterson, D.M., Clarke, L.L., Mrsny, R.J., and Turner, J.R. (2005). Epithelial myosin light chain kinase-dependent barrier dysfunction mediates T cell activation-induced diarrhea in vivo. J. Clin. Invest. *115*, 2702–2715.

Clemente, J.C., Ursell, L.K., Parfrey, L.W., and Knight, R. (2012). The impact of the gut microbiota on human health: an integrative view. Cell *148*, 1258–1270.

Denison, M.S., and Nagy, S.R. (2003). Activation of the aryl hydrocarbon receptor by structurally diverse exogenous and endogenous chemicals. Annu. Rev. Pharmacol. Toxicol. *43*, 309–334.

Dong, F., Zhang, L., Hao, F., Tang, H., and Wang, Y. (2013). Systemic responses of mice to dextran sulfate sodium-induced acute ulcerative colitis using H NMR spectroscopy. J. Proteome Res. *12*, 2958–2966.

Ettarh, R.R., and Carr, K.E. (1996). Morphometric analysis of the small intestinal epithelium in the indomethacin-treated mouse. J. Anat. *189*, 51–56.

Fasano, A., and Shea-Donohue, T. (2005). Mechanisms of disease: the role of intestinal barrier function in the pathogenesis of gastrointestinal autoimmune diseases. Nat. Clin. Pract. Gastroenterol. Hepatol. *2*, 416–422.

Gummesson, A., Carlsson, L.M., Storlien, L.H., Bäckhed, F., Lundin, P., Löfgren, L., Stenlöf, K., Lam, Y.Y., Fagerberg, B., and Carlsson, B. (2011). Intestinal permeability is associated with visceral adiposity in healthy women. Obesity (Silver Spring) *19*, 2280–2282.

Gupta, N.K., Thaker, A.I., Kanuri, N., Riehl, T.E., Rowley, C.W., Stenson, W.F., and Ciorba, M.A. (2012). Serum analysis of tryptophan catabolism pathway: correlation with Crohn's disease activity. Inflamm. Bowel Dis. *18*, 1214–1220.

Hart, M.L., Ceonzo, K.A., Shaffer, L.A., Takahashi, K., Rother, R.P., Reenstra, W.R., Buras, J.A., and Stahl, G.L. (2005). Gastrointestinal ischemia-reperfusion injury is lectin complement pathway dependent without involving C1q. J. Immunol. *174*, 6373–6380.

Hisamatsu, T., Okamoto, S., Hashimoto, M., Muramatsu, T., Andou, A., Uo, M., Kitazume, M.T., Matsuoka, K., Yajima, T., Inoue, N., et al. (2012). Novel, objective, multivariate biomarkers composed of plasma amino acid profiles for the diagnosis and assessment of inflammatory bowel disease. PLoS ONE *7*, e31131.

Islam, S.A., and Luster, A.D. (2012). T cell homing to epithelial barriers in allergic disease. Nat. Med. *18*, 705–715.

Jansson, J., Willing, B., Lucio, M., Fekete, A., Dicksved, J., Halfvarson, J., Tysk, C., and Schmitt-Kopplin, P. (2009). Metabolomics reveals metabolic biomarkers of Crohn's disease. PLoS ONE *4*, e6386.

Kelly, D., Campbell, J.I., King, T.P., Grant, G., Jansson, E.A., Coutts, A.G., Pettersson, S., and Conway, S. (2004). Commensal anaerobic gut bacteria attenuate inflammation by regulating nuclear-cytoplasmic shuttling of PPAR-gamma and RelA. Nat. Immunol. *5*, 104–112.

Leavy, O. (2011). Mucosal immunology: the 'AHR diet' for mucosal homeostasis. Nat. Rev. Immunol. *11*, 806.

Lee, K.A., Kim, S.H., Kim, E.K., Ha, E.M., You, H., Kim, B., Kim, M.J., Kwon, Y., Ryu, J.H., and Lee, W.J. (2013). Bacterial-derived uracil as a modulator of mucosal immunity and gut-microbe homeostasis in *Drosophila*. Cell *153*, 797–811.

Lin, H.M., Barnett, M.P., Roy, N.C., Joyce, N.I., Zhu, S., Armstrong, K., Helsby, N.A., Ferguson, L.R., and Rowan, D.D. (2010). Metabolomic analysis identifies inflammatory and noninflammatory metabolic effects of genetic modification in a mouse model of Crohn's disease. J. Proteome Res. *9*, 1965–1975.

Lu, K., Knutson, C.G., Wishnok, J.S., Fox, J.G., and Tannenbaum, S.R. (2012). Serum metabolomics in a Helicobacter hepaticus mouse model of inflammatory bowel disease reveal important changes in the microbiome, serum peptides, and intermediary metabolism. J. Proteome Res. *11*, 4916–4926.

Maloy, K.J., and Powrie, F. (2011). Intestinal homeostasis and its breakdown in inflammatory bowel disease. Nature *474*, 298–306.

Martin, F.P., Wang, Y., Sprenger, N., Yap, I.K., Rezzi, S., Ramadan, Z., Peré-Trepat, E., Rochat, F., Cherbut, C., van Bladeren, P., et al. (2008). Top-down systems biology integration of conditional prebiotic modulated transgenomic interactions in a humanized microbiome mouse model. Mol. Syst. Biol. *4*, 205.

Matsui, H., Shimokawa, O., Kaneko, T., Nagano, Y., Rai, K., and Hyodo, I. (2011). The pathophysiology of non-steroidal anti-inflammatory drug (NSAID)-induced mucosal injuries in stomach and small intestine. J. Clin. Biochem. Nutr. *48*, 107–111.

Mayer, E.A. (2011). Gut feelings: the emerging biology of gut-brain communication. Nat. Rev. Neurosci. *12*, 453–466.

Meier, C., and Plevy, S. (2007). Therapy insight: how the gut talks to the joints—inflammatory bowel disease and the spondyloarthropathies. Nat. Clin. Pract. Rheumatol. *3*, 667–674.

Mukherji, A., Kobiita, A., Ye, T., and Chambon, P. (2013). Homeostasis in intestinal epithelium is orchestrated by the circadian clock and microbiota cues transduced by TLRs. Cell *153*, 812–827.

Musch, M.W., Clarke, L.L., Mamah, D., Gawenis, L.R., Zhang, Z., Ellsworth, W., Shalowitz, D., Mittal, N., Efthimiou, P., Alnadjim, Z., et al. (2002). T cell activation causes diarrhea by increasing intestinal permeability and inhibiting epithelial Na+/K+-ATPase. J. Clin. Invest. *110*, 1739–1747.

Patel, R.M., Myers, L.S., Kurundkar, A.R., Maheshwari, A., Nusrat, A., and Lin, P.W. (2012). Probiotic bacteria induce maturation of intestinal claudin 3 expression and barrier function. Am. J. Pathol. *180*, 626–635.

Rath, C.M., and Dorrestein, P.C. (2012). The bacterial chemical repertoire mediates metabolic exchange within gut microbiomes. Curr. Opin. Microbiol. *15*, 147–154.

Roger, T., Froidevaux, C., Le Roy, D., Reymond, M.K., Chanson, A.L., Mauri, D., Burns, K., Riederer, B.M., Akira, S., and Calandra, T. (2009). Protection from lethal gram-negative bacterial sepsis by targeting Toll-like receptor 4. Proc. Natl. Acad. Sci. USA *106*, 2348–2352.

Salzman, N.H. (2011). Microbiota-immune system interaction: an uneasy alliance. Curr. Opin. Microbiol. *14*, 99–105.

Turner, J.R. (2009). Intestinal mucosal barrier function in health and disease. Nat. Rev. Immunol. *9*, 799–809.

Van Itallie, C.M., and Anderson, J.M. (2006). Claudins and epithelial paracellular transport. Annu. Rev. Physiol. *68*, 403–429.

Wang, K., Damjanov, I., and Wan, Y.J. (2010). The protective role of pregnane X receptor in lipopolysaccharide/D-galactosamine-induced acute liver injury. Lab. Invest. *90*, 257–265.

Wang, H., Venkatesh, M., Li, H., Goetz, R., Mukherjee, S., Biswas, A., Zhu, L., Kaubisch, A., Wang, L., Pullman, J., et al. (2011). Pregnane X receptor activation induces FGF19-dependent tumor aggressiveness in humans and mice. J. Clin. Invest. *121*, 3220–3232.

Watkins, R.E., Wisely, G.B., Moore, L.B., Collins, J.L., Lambert, M.H., Williams, S.P., Willson, T.M., Kliewer, S.A., and Redinbo, M.R. (2001). The human

nuclear xenobiotic receptor PXR: structural determinants of directed promiscuity. Science *292*, 2329–2333.

Weiser, M.M. (1973). Intestinal epithelial cell surface membrane glycoprotein synthesis. II. Glycosyltransferases and endogenous acceptors of the undifferentiated cell surface membrane. J. Biol. Chem. *248*, 2542–2548.

Wells, J.M., Rossi, O., Meijerink, M., and van Baarlen, P. (2011). Epithelial crosstalk at the microbiota-mucosal interface. Proc. Natl. Acad. Sci. USA *108* (*Suppl 1*), 4607–4614.

Wikoff, W.R., Anfora, A.T., Liu, J., Schultz, P.G., Lesley, S.A., Peters, E.C., and Siuzdak, G. (2009). Metabolomics analysis reveals large effects of gut microflora on mammalian blood metabolites. Proc. Natl. Acad. Sci. USA *106*, 3698–3703.

Xavier, R.J., and Podolsky, D.K. (2007). Unravelling the pathogenesis of inflammatory bowel disease. Nature *448*, 427–434.

Yamaguchi, A., Hori, O., Stern, D.M., Hartmann, E., Ogawa, S., and Tohyama, M. (1999). Stress-associated endoplasmic reticulum protein 1 (SERP1)/Ribosome-associated membrane protein 4 (RAMP4) stabilizes membrane proteins during stress and facilitates subsequent glycosylation. J. Cell Biol. *147*, 1195–1204.

Zhou, C., Tabb, M.M., Nelson, E.L., Grün, F., Verma, S., Sadatrafiei, A., Lin, M., Mallick, S., Forman, B.M., Thummel, K.E., and Blumberg, B. (2006). Mutual repression between steroid and xenobiotic receptor and NF-kappaB signaling pathways links xenobiotic metabolism and inflammation. J. Clin. Invest. *116*, 2280–2289.